Nonlin. Processes Geophys. Discuss., 1, 97–129, 2014
www.nonlin-processes-geophys-discuss.net/1/97/2014/
doi:10.5194/npgd-1-97-2014

Nonlinear Processes in Geophysics
Discussions
Open Access

On modulation instability in a system of jets, waves and eddies off California

L. M. Ivanov[1], **C. A. Collins**[1,2], **and T. Margolina**[1]

[1]Naval Postgraduate School, Monterey, California, USA
[2]Moss Landing Marine Laboratories, Moss Landing, California, USA

Received: 31 January 2014 – Accepted: 3 February 2014 – Published: 20 February 2014

Correspondence to: L. M. Ivanov (lmivanov@nps.edu)

Published by Copernicus Publications on behalf of the European Geosciences Union & American Geophysical Union.

Abstract

SSH altimetry observations for 1992 to 2009 off Central and Southern California are used to show that observed quasi-zonal jets were likely driven by near-resonance interactions between different scales of the flow. Quartet (modulational) instability dominated and caused non-local transfer of energy from waves and eddies to bi-annual oscillations and quasi-zonal jets. The total number of quartets induced off California was approximately 10 times larger than the number of existing triads, and quartet amplitudes in general were larger than triad amplitudes. The spectral centroid regularly shifted into the domain of low-order modes. Local "negative" viscosity probably did not generate a classical inverse cascade because the spectrum of SSHs did not demonstrate power behavior. Two types of quartets were identified: (a) quasi-zonal jets, annual and semi-annual Rossby waves and eddies, and (b) bi-annual oscillations, semi-annual Rossby waves and eddies. For a case with bottom friction, quartet instability required the existence of a certain level of dissipativity in the flow.

1 Introduction

In recent years there has been growing recognition of the existence of persistent quasi-zonal jets (QZJs) in the mid-latitude atmosphere as well as in the atmospheres of gaseous planets (an intensive review of QZJs is given by Baldwin et al. (2007). These jets were clearly detected in the atmospheres of planets and Earth because they were intense and had a clear signature in cloud systems. This is not the case for the Earth's oceans because oceanic QZJs are latent (i.e., masked by more intense non-zonal flows), and can only be extracted from observations and model results by statistical procedures. Therefore, the role of QZJs in ocean dynamics and the nature of these jets are not clear due to their weak signal.

A number of the generation of QZJs includes: modulation instability, β-plumes, inverse cascade and others. Most results were derived from analysis of 2-D models

NPGD
1, 97–129, 2014

of QZJs which yielded useful analytical results (Loesch, 1977; Newell, 1969; Rhines, 1975; Vallis and Maltrud, 1991; Nadiga, 2006; Galperin et al., 2010; Connaugton et al., 2010; Wang et al., 2012 among others). However these results were obtained for simplified jet models, and it is difficult to use these models to detect mechanisms of oceanic jet generation which might exist in nature.

Srinivasan and Young (2012) demonstrated that zonal jets could be reproduced with a linear theory and did not rely upon the existence of an inverse cascade. The results presented here do not agree with Srinivasan and Young (2012) because in our opinion nonlinearity played a very important role in the jet generation; therefore, results were not compared to those obtained by Srivistan and Young (2012).

A number of alternative hypotheses based on 3-D models, have been proposed to explain the QZJs (see Hristova et al., 2008; Berloff et al., 2009, 2011; Wang et al., 2012 among others). For example, Hristova et al. (2008) hypothesized that QZJs, observed in the eastern region of subtropical gyres may be related to radiating instabilities of eastern boundary currents.

Connaugton et al. (2010) have suggested using a modulational instability concept for explanation of quasi-zonal jets observed in the ocean and atmosphere. Connaugton et al. (2010) found that in a 2-D case for very weak primary waves, the unstable waves were close to being in three-wave resonance with the primary waves. They have revised the linear theory of Gill (1974) using a 4-mode truncation and emphasized the role of the carrier amplitude/nonlinearity, the role of the deformation radius and the role of resonant wave interactions in the case of a stronger nonlinear carrier wave.

Ivanov et al. (2010) demonstrated that annual and semi-annual Rossby waves could be interpreted as weak nonlinear waves because their nonlinearity parameters changed by as much as several units. They used a zonal component of propagation speed (which varied from zero to several cm s^{-1}), the wave steepness, q, ($0 < q < 2-3$), and the length of spatial phase coherence for detection of different regimes of Rossby wave evolution. It follows that nonlinear interactions between these waves

NPGD
1, 97–129, 2014

should be studied with a view to understanding whether and how they might influence quasi-zonal jets.

This study analyses SSH observations off California and shows that

a. mesoscale flow off California was driven by near-resonance interactions between flow scales. Four wave near-resonance interactions between spatial scales dominated and formed specific structures of the mesoscale flow including a combination of QZJs, biannual oscillations, annual Rossby waves, semi-annual Rossby waves and mesoscale eddies of smaller scales;

b. the SSH signal was transferred from Rossby waves (RWs) and mesoscale eddies (MEs) to lower-frequency currents (biannual oscillations – BAOs – and QZJs). The existence of two different quartets was found: QZJ-annual RWs- semi-annual RWs-MEs and BAOs-semi-annual RWs-MEs of two different scales. However for both these quartets, the SSH signal was pumped from faster to slower scales;

c. QZJ (or BAO) generation by modulational instability required the existence of a certain level of dissipativity in mesoscale flows. Dissipativity played an important role because it determined a number of possible near-resonance interactions as well as the latency of observed QZJs.

In general, the dimensionality of analyzed QZJs cannot be based on the analysis of SSHs only. However, QZJs are shown to be dissipative structures and their generation was the result of a self-organization process. Following Nicolis and Prigogine (1977), dissipative structures are defined as non-equilibrium thermodynamic systems that generate order spontaneously by exchanging energy with their external environment. Self-organization is generation of regular structures in far-from-equilibrium states of a dissipative system due to interactions of the elements that make up the system (Nicolis and Prigogine, 1977).

The remainder of the paper is organized as follows. Section 2 describes the data and methods used. A system of jets (waves and eddies reconstructed from AVISO

NPGD
1, 97–129, 2014

products) is discussed in Sect. 3. Robustness and repetition of QZJ generation are demonstrated in Sect. 3. Sections 4 and 5 include calculation of near resonance and resonance interactions off Central California. The re-distribution of surface elevation between different scales and scales dominating the surface elevation are discussed in Sect. 6. Although Sect. 6 is simply a kinematic analysis, it is shown that energy was pumped from Rossby waves and mesoscale eddies to QZJs and BAOs. The role of dissipativity in the process of energy re-distribution is discussed in Sect. 7. Section 8 shows how different scales forming quasi-zonal jets and bi-annual oscillations were grouped in separate quartets. Conclusions are given in Sect. 9.

2 Data and methods

The SSH anomaly field was produced by the AVISO Project (Archiving Validation and Interpretation on Satellite Data in Oceanography) for the period from 10 October 1992 to 23 May 2009 (Collecte Localisation Satellites, 2006). To understand the spatio-temporal complexity of altimetry signals, a double spectral approach (DSA) (Ivanov and Collins, 2009) was applied to the analysis of the SSH anomaly field. Following this approach, the SSH anomaly field $\eta(\boldsymbol{x}, t)$ is represented by

$$\eta(\boldsymbol{x}, t) = \sum_{m=1}^{M} a_m(t)\Psi_m(\boldsymbol{x}), \tag{1}$$

where $\boldsymbol{x} = (x, y)$ is the position vector in a real-space, Ψ_m are basis functions (or M-modes which extend the classical Fourier polynomials to nonrectangular basins) calculated as in Ivanov and Collins (2009). Note that $\Psi_m(\boldsymbol{x}) = \sum_{l=1}^{L} c_{lm} \sin(kx/L_x)\sin(ky/L_y)$ only for a rectangular basin. Here L_x and L_y are horizontal basin scales, $k = 2\pi/l$. Figure 1 shows the structure of several basis functions for the observational region. About

1000 basis functions were used to represent SSH with less than 1 % rmse. Different combinations of basis functions formed currents which had different spatial scales.

The spectral coefficients a_m were then analysed using a discrete wavelet transform as

$$a_{\mathrm{m}j}(t) = \sum_{p=1}^{\infty} b_{\mathrm{m},j,p} T_{j,p}(t), \tag{2}$$

where $a_{\mathrm{m}j}$ is an approximation of a_m with resolution j, $T_{j,p} = 1/2^{j/2}\varphi(2^j t - p)$, and φ is the father wavelet. Finally, results were summed around selected time scales j using Eq. (1).

A Debaucher 6th order wavelet transform was used in this study. This allowed for the introduction of six frequency bands (FBs) centered on the frequencies (ϖ_p) calculated by Laskar's method (Laskar, 1993): (1) 1 to 2 months (referred to as the mesoscale eddy II (MEs-II) band), (2) 2 to 4 months (ME-I band), (3) 4 to 8 months (semiannual Rossby waves or SARW band), (4) 8 to 18 months (annual Rossby waves or ARW band), (5) 18 to 36 months (bi-annual oscillations or BAO band) and (6) longer than 36 months (quasi-zonal jets or QZJ band). Coherent mesoscale structures (jets, propagating waves and eddies) were selected within these six frequency bands and for a spatial spectral band limited by the 30th (lower boundary) and 250th (upper boundary) M-modes.

Calculations should be robust for the choice of upper and lower boundaries: the results did not change when the upper boundary of the band was moved toward higher-order modes, but changed weakly when the lower boundary was moved to the 15th mode. As discussed in Ivanov et al. (2010), modes from 1 to 29 were responsible for large-scale seasonal variability and therefore were not included in the analyses.

Similarly, variations in observational sampling should not affect coherent (long-lived) structures. The length of observational sampling was reduced 4–6 times without changing the structure of quasi-jets. This was a consequence of using the Debaucher wavelet transform for the spectral representation of spectral coefficients a_m.

3 A system of jets, waves and eddies off California

The mesoscale coherent structures observed in SSH observations off California shared overlapping spatial scales but distinct time scales. This allowed for detection and selection of QZJs, BAOs, RWs and MEs. Time-averaged spectra for each of the six frequency bands are shown in Fig. 2a and b as a function of mode number. Figure 2a shows that the SSH signal was very small for $m > 250$ and that QZJs were considerably weaker than annual RW. Figure 2b indicates that BAO were weaker than semi-annual RW. Explicit peaks for spectrum a_m^2 were observed for all frequency bands (Fig. 2a and b) within the domain bounded by 30th and 250th M-modes. This indicated the existence of energy-dominant scales in the mesoscale flow. The instantaneous spectra were very rough with multiple narrow peaks (Fig. 2c). The instantaneous spectrum structure was similar to those observed in weakly nonlinear flows (Rabinovich and Trubetskov, 1989).

Characteristic spatial structures for all six frequency bands of the current system are shown in Fig. 3a–f. The coherent structures shown in Fig. 3 for the different frequency bands differed from one another and were not stationary. Temporal behavior is discussed below.

QZJs represented eddy chains stretched from east to west and each chain appeared as a number of eddies of the same sign embedded in an envelope of less intensive zonal shear flow (Fig. 3a). SSH in the jets reached 4–5 cm and was not less than 2.5–3 cm within the 17 yr observational period. The ratio of zonal and meridional scales for the QZJs ($R = L_{\text{zonal}}/L_{\text{merid}}$) varied from 2–3 (short jets) to 7–8 (long jets). Odd M-modes dominated Eq. (1) which resulted in anisotropy of the QZJ envelope. Direction of QZJ axes varied from west to southwest. The QZJs also moved equatorward with speed of as great as 0.2 cm s^{-1}. However, there was no zonal motion associated with the southward movement. Results clearly indicated that QZJs were regular structures with robust recurrence and could not be interpreted as statistical fluctuations.

BAOs did not demonstrate any steady motion to either west or southwest and their shape differed somewhat from QZJs (Fig. 3b). The structure of BAOs was often close to the structure of standing waves and therefore they were interpreted as quasi-standing waves. The oscillations were more stronger than for QZJs. SSHs for BAOs reached ~ 5–7 cm.

Propagating RWs with annual and semi-annual periodicities were detected and are shown in Fig. 3c and d. Jacobs et al. (1993, 1996) had identified semiannual linear Rossby waves and semiannual oscillations in the Pacific Ocean from satellite data for latitudes as high as to 35 and 45° N, respectively, when barotropic and first baroclinic modes were fitted to Geosat data. Ivanov et al. (2012b) have analyzed satellite data in the Pacific Ocean within a region from 7 to 60° N and found semiannual Rossby waves south of 45° N. These waves were nonlinear for most of their existence, i.e. they had relatively large steepness (see, for example, Rhines, 2002, 2004).

The annual and semiannual RWs dominated the mesoscale flow off California because SSHs for the waves reached ~ 10–12 cm. The Rossby waves demonstrated robust recurrence in a sequence of dynamical regimes: linear, amplification and saturation. Figure 3c and d show the spatial structure for annual and semi-annual Rossby waves on 4 October 2006, and 28 November 2007, respectively. The waves propagated westward and southwestward. The propagation speed varied with time and had maximum values in the linear regime of up to 7–10 cm s^{-1} and minimum value in the saturation regime when a halt of westward wave propagation was observed. Semi-annual waves were more anisotropic than annual waves (compare Fig. 3c to d). Comparing alongshore (L_h) and across shore (L_n) spatial scales, annual Rossby waves were characterized by $L_n \sim L_h$ or $L_n > L_h$. For semi-annual Rossby waves $L_h \gg L_n$. The structure of semi-annual waves was close to meridional. Further discussion of the behavior of the Rossby waves can be found in Ivanov et al. (2010).

MEs-I and MEs-II with scales smaller than RWs were also observed off California (Fig. 3e and f). They formed an eddy field which was statistically inhomogeneous across-shore and demonstrated mean propagation from the coast to the west or

NPGD
1, 97–129, 2014

southwest. SSH for these eddies reached several cm. To distinguish Rossby waves and mesoscale eddies, the spatial phase coherence criterion (spatial correlation of the phase of the SSH field) was used [Ivanov et al., 2010].

Several features of the coherent structures observed off California were important for the present analysis. First, all structures were generally weakly nonlinear excluding the cases when $\left\langle \eta^2(t) \right\rangle = \int \int \eta^2(x, y, t)\,\mathrm{d}x\,\mathrm{d}y$ reached maximal and minimal values (Fig. 4). Here, integration was over the computational domain starting on 10 October 1992. Maximum values corresponded to periods when wave steepness $q \sim 2$ (transition to turbulence regime), and minimal values to $q \ll 1$ (linear structures). Interplay between different M-modes was easily detected via the frequency-phase analysis of M-mode structures in phase space (not shown). The interplay between M-modes will be shown through the analysis of triplets and quartets in the next sections.

Second, the behavior of $\left\langle \eta^2(t) \right\rangle$ with time showed robustness for the studied process (Fig. 4). For all six spectral bands, the behavior of this function was robust with time. Here robustness is a repetition of certain dynamical regimes. Maxima for QZJs corresponded to minima of $\left\langle \eta^2 \right\rangle$ for BAOs.

Third, a low-frequency modulation (not modulation instability) was visible by eye for all spectral bands shown in Fig. 4 (Rabinovich and Trybetskov, 1993). This modulation became stronger for higher-order spectral bands.

4 Wavelet analysis

RWs and QZJs demonstrated nonlinear behavior. The observed RW steepness was finite (most of the time the steepness was ≤ 1) and the QZJs consisted of chains of eddies which stretched from east to west. These eddy chains may indicate the importance of nonlinear dynamics (see for example, Dritschell and Scott, 2011). Thus it is logical to study nonlinear mechanisms of QZJ generation and evolution. Numerical and theoretical studies (Gill, 1974; Lee and Smith, 2007 and others) demonstrated that quasi-zonal jets can be generated by resonance as well as near-resonance interactions between flow scales in simplified models.

These interactions should be detected in a phase space which embeds altimetry SSH signals. M-modes were used as a basis to form an appropriate phase space. Next phase-frequency analysis of M-mode (wave) dynamics was carried out using amplitude (W_m) and phase (ϕ_m). Both variables, W_m and ϕ_m, were determined for each M-mode using the Morlet wavelet transform (ψ_τ),

$$W_\mathrm{m}(\tau,t) = |W_\mathrm{m}(\tau,t)| \exp\{i\,\phi_\mathrm{m}(\tau,t)\}, \tag{3}$$

where $W_\mathrm{m}(\tau,t) = \int\limits_{-\infty}^{+\infty} a_\mathrm{m}(t')\,\psi_\tau^*[(t-t')/\tau]\,\mathrm{d}t'$, τ is a time scale, and $\omega(m) = \frac{\mathrm{d}\phi_\mathrm{m}}{\mathrm{d}t}$ is instantaneous frequency (for details of wavelet techniques see Kumar and Foufoula-Georgiou, 1997).

The absolute value of the amplitude $|W_\mathrm{m}|$ describes the evolution of energy-dominant peaks at certain time scales (or frequencies) ($|W_\mathrm{m}|^2$ is also called the wavelet power spectrum, which in contrast to the Fourier power spectrum, is a function of time). Given the length of the observational series (nearly 17 yr), statistically significant estimates of wavelet amplitude can be obtained for a domain bounded by 1 month $\leq \tau \leq$ 6 yr and 8 yr $\leq t \leq$ 12 yr (Kumar and Foufoula-Gergiou, 1997).

Energy-dominant peaks were detected by examining the structure $|W_\mathrm{m}|$. The peaks were selected as to satisfy one of the following conditions.

Three m modes participated in near-resonance interactions and formed an appropriate triplet mode if

$$m + k = l, \quad |\omega(m) + \omega(k) - \omega(l)| \leq \Omega_1. \tag{4}$$

Four modes were members of a mode quartet if

$$m + k = l, \quad |\omega(m) + \omega(k) - \omega(l)| \leq \Omega_1, \tag{5}$$

$$n - m = l, \quad |\omega(n) - \omega(m) - \omega(l)| \leq \Omega_2. \tag{6}$$

Here Ω_1 and Ω_2 represent resonance broadenings which are caused by finite nonlinearity. Nonlinear interactions are effective if $\Omega_1, \Omega_2 \leq \Gamma_m$, where Γ_m is the inverse of the characteristic time of nonlinear evolution of the mth mode (Janseen, 2003; Kartashova et al., 2010, and others). For resonance interactions – $\Omega_1 = \Omega_2 = 0$.

Conditions (Eqs. 5 and 6) are able to describe modulation instability when the lth mode of RW, two mth and nth modes (similar to sideband waves) and the *k*th mode of lower frequency flow interact with one another in nonlinear sense (Manfredi et al., 2001). Note that conditions (Eqs. 5 and 6) have to be met during a specific time interval because either all modes in a quartet fail to exist after nonlinear interactions or all modes continue to exist in quartets but quartets become unstable and decay due to inhomogeneity of the background flow, vertical temperature gradients etc.

Since many of near resonance quartets and triplets lived as long as 14 days or longer, as estimated from analysis of the wavelet power spectrum, it was possible to estimate how surface elevation was re-distributed between different scales and in particular between m-modes for frequency bands corresponding to QZJs, RWs and eddies. Superposition of RW and eddy m-modes (see Eq. 4) results in growth of QZJ mode, identified from the analysis of time evolution of all three m-modes (Eq. 4) which are a part of a quartet. Quartets with growth of m-modes (within a mean lifetime) corresponding to QZJs showed that a SSH was re-distributed from high to low frequency m-modes. This was a rough estimate because a part of short-lived m-modes with lifetimes less than 14 days were excluded from our analysis,

Conditions (Eqs. 4–6) corresponded to near-resonance nonlinear interactions described by the Poisson bracket $\{\eta, \Delta\eta\}$ for quasi-geostrophic flows or $\{\Psi, \eta\}$ without the geostrophic approximation (Ψ is "a stream" function) (Pedlosky, 1987). The "stream" function can be defined through a two scalar potential representation of a three-dimensional incompressible flow. See, for example, Moffatt (1978) or Chu et al. (2003) for applications. Obviously, in this case the two scalar potentials Ψ and Φ defined here are not the same as the stream function and velocity potential of a two-dimensional flow (this is discussed in Chu et al., 2003). The statistical stability needed

NPGD
1, 97–129, 2014

for detection of triads and quartets was achieved through special smoothing with a priori constraints applied (Ivanov et al., 2012a).

Note that horizontal velocity was not estimated from SSH using geostrophic relationships because non-geostrophic motions in the studied coastal oceanic area may contain up to 30 % of the total kinetic energy of horizontal circulation (Marchesiello et al., 2003) and frontal dynamics plays an important role in forming circulation in the California Current system (Castelao et al., 2006).

For this study, triads were detected which satisfied Eq. (5) as the first step, and then checked to see if two m-modes from this triad formed a second triad (Eq. 6). If the second triad was [not] found, the existence of quartet (Eqs. 5–6) (triad Eq. 4) was confirmed. Figure 5a and b shows a resonance triad (a) and near-resonance quartet (b). In both these cases, energy was transferred to low-frequency time scales. The number of possible near-resonance triads and quartets participating in nonlinear interactions were defined by the choice of resonance broadening.

Note that to understand energy re-distribution within the energy spectrum, the energy transfer integrals need to be calculated (for example, see Sagau and Cambon, 2008). Unfortunately that cannot be done because equations describing SSH anomaly motions contain terms which cannot be determined from satellite altimetry data only. Therefore simpler characteristics were calculated which described the re-distribution of the altimetry signal between scales (see Sect. 6). This approach allowed calculation of general characteristics of the re-distribution of energy. Generally, "inverse" transfer from fast motions to slower motions was observed but not from small to large spatial scales.

Triplet and quartet interactions showed different mechanisms of energy re-distribution between scales and as well as different time scales for generation of QZJs. For example, Loesch (1977) demonstrated that the time scale required for jet generation by quartet interactions was an order of magnitude longer than that associated with triad interactions.

NPGD
1, 97–129, 2014

L. M. Ivanov et al.

Title Page
Abstract | Introduction
Conclusions | References
Tables | Figures
◀| |▶
◀ ▶
Back | Close
Full Screen / Esc
Printer-friendly Version
Interactive Discussion

5 Resonance and near-resonance interactions

On average, between 1999 and 2003, at each moment in time, ~40–80 resonance triads ($\Omega_1 = 0$), ~3–5 resonance quartets ($\Omega_1 = 0$, $\Omega_2 = 0$), about 2×10^4 near-resonance triads ($0 < \Omega_1 < \Omega^*$) and 1.75×10^5 near-resonance quartets ($0 < \Omega_1 < \Omega^*$, $0 < \Omega_2 < \Omega^{**}$) were detected (see Fig. 6). For simplicity, hereafter, $\Omega^* < \Omega^{**} = 0.01$ radians. The number of triads and quartets changed with time but not very quickly (Fig. 5a). The number of quartets decreased as $\Omega^* \sim \Omega^{**} \to 0$, but was always larger than the number of triads if $\Omega^{**} > \Omega_{cr}$ for reasonable values of resonance broadening (Fig. 5b).

The stability of resonance quartets and triads depends on the inhomogeneity of the background conditions of the ocean (density gradient, shear flow, etc.). This inhomogeneity should destroy exact resonances, and most likely exact resonances dominate only in simplified theoretical models. Therefore, in mesoscale oceanic flows, near-resonance interactions are more likely. The intensity of these interactions is determined by the resonance broadening and kinematic features of near resonances.

Squared amplitudes for most quartets were also larger (some amplitudes were much larger) than the squared amplitudes of triads (not shown). The dominance of near-resonant quartets compared to resonant and near-resonant triads indicated that there was modulation instability of Rossby waves off California: modulations of the Rossby wave envelope excited zonal flows through a nonlinear mechanism (probably Reynolds stress).

The number of near resonance quartets (N^{q}) and the number of near resonance triads (N^{tr}) did not change much with time (Fig. 5a). Quartets dominated off Central California. N^{q} was much larger than N^{tr} except for values of $\Omega \ll 0.01$ radians (Fig. 5b). Squared amplitudes, a_m^2, for most quartets were also larger (some amplitudes were much larger) than the squared amplitudes of triads (not shown).

NPGD
1, 97–129, 2014

6 Re-distribution of surface elevation between scales

Kinematic analysis was applied to understand how mean squared SSH was re-distributed between different scales. The number of quartets for which a signal was transferred from waves and eddies to QZJs and BAOs is shown in Fig. 6a. (Note that this number was considerably less than the total number of existing quartets shown in Fig. 5a). This indicated a dominant role for four-wave interactions (modulational instability) in the process of forming SSH spectra as compared to three-wave interactions.

M-modes for QZJs and BAOs had mean time scales of 4.3 ± 0.7 yr and 2.4 ± 0.9 yr, respectively (Fig. 6b). Variations of both mean time scales were not large, which reflected a high degree of regularity of QZJs and BAOs off California.

Since the wave steepness, q, can be larger than 1 for quite short time periods associated with a transition to turbulence, under some conditions an inverse cascade can occur or coexist with modulational instability. Naturally when $q \ll 1$, pure modulational instability dominates (Connaughton et al., 2010). Therefore it is important to look for the existence of an inverse cascade in our analyses.

Two criteria were used to determine and identify whether or not an inverse cascade formed QZJs. First, spectral entropy was used to estimate the re-distribution of SSH signals between different m-modes (Aubry et al., 1991). The spectral entropy, S, was calculated as

$$S(M,t) = -(\log M)^{-1} \sum_{m=m_o}^{M} p_\mathrm{m} \log p_\mathrm{m}, \tag{7}$$

where $p_\mathrm{m}(t) = a_\mathrm{m}^2/a(t)$; $a(t) = \sum\limits_{m=m_o}^{M} a_\mathrm{m}^2(t)$, equals one for a uniform distribution of a signal among all $(M - m_0)$ modes and equals zero when the signal was contained in a single mode.

Figure 7a shows the behavior of $S(M,t)$ with time for modes numbered from $m_0 = 30$ to $M = 250$. This figure shows that there was no explicit signal flux from small scales to

NPGD
1, 97–129, 2014

large scales of SSH during the entire observational period. $S(M,t)$ fluctuated from 0.68 to 0.72. Increasing M to 1000 increased the mean value of S only slightly to 0.72. These results indicated that either there was no inverse cascade of energy or that the cascade was weak.

The centroid for spectrum of η^2 from $m_0 = 30$ to $M = 1000$ was also calculated to identify inverse cascade. Figure 7b demonstrates the behavior of the spectral centroid with time. A simple analysis of this behavior is that there were time intervals within which the centroid shifted to larger scales. To illustrate the character of this shift, the spectrum of a_m^2 for day 2940 (point A on Fig. 8a) when the centroid was 82 (Fig. 8b) was contrasted with the spectrum on day 3150 (point B on Fig. 8a) when the centroid had decreased to 62 (Fig. 8c). The spectra after the shift (Fig. 8c) showed a decay of energy for M-modes with $m > 100$. From another perspective, η_m^2 did not demonstrate a power behavior with m (not shown). This indicated that the classical inverse cascade was not observed in our analysis of the satellite data. A specific mechanism for the reduction of the spectral centroid position will be studied in another paper. It may be caused by three dimensional or other effects.

The mechanism of QZJ generation due to near-resonance inter-scale interactions is similar to that suggested by Lorenz (1972) for barotrophic flow, and was originally called "Rossby wave instability" by Lorenz. A finite-amplitude Rossby wave interacts with a zonal flow perturbation on a β-plane. The surfaces of constant phase move to the west. The zonal flow tends to distort them. At this point, it is easy to see that the waves being transverse, fluid particles, whose velocity is parallel to the wave front, need to turn to the west. This imparts eastward momentum when the fluid particles cross the zonal flow perturbation. This continuous deposition of eastward momentum by the wave produces a positive feedback mechanism leading to exponential growth of the zonal perturbation.

However, in contrast to Lorenz (1972), modulational instability dominated the mesoscale flow off California and there was channeling of energy not only to QZJs but also to BAOs. This is a typical self-organized process. Energy was pumped by wind into the ocean and then it was re-distributed between scales so that robust regular structures (QZJs and BAOs) were formed due to nonlinear interactions between scales (Nicolis and Prigogine, 1977).

7 Role of flow dissipativity

Lee and Smith (2007) suggested that the resonance broading $\Omega = \gamma \cdot Rn$, where γ is a small parameter and Rn is a non-dimensional Rhines number, the latter defined for the β-plane system as the ratio of linear and nonlinear time scales. With characteristic length scale L and nonlinear time scale L/U, the Rhines number is equal to $U/(L^2\beta)$. The resonance broadening seen above is determined by the dissipativity of mesoscale flow caused by bottom friction, vertical viscosity, etc. The Rhines scale depends on the level of dissipativity and inhomogeneity of the background medium (density gradient, shear flow etc.) (Danilov and Gurarie, 2002). This inhomogeneity should destroy exact resonances, and exact resonances probably dominate only for simplified theoretical models. Near-resonance interactions seem more likely for mesoscale oceanic flows. Intensity of near-resonance interactions is determined by resonance broadening and kinematic features of near resonances.

Therefore, dissipativity of mesoscale flow should play an important role in redistribution of energy between scales because its level determines the number of near resonances involved in energy exchange between scales. This can be illustrated by assuming that linear bottom friction with coefficient λ dominated the mesoscale flow. The Rhines number is defined as

$$Rn \sim \beta^{-1}\lambda^{-1/2}\varepsilon^{1/2}L^{-1} \tag{8}$$

where β and ε are gradients of the local Coriolis parameter and injection rate, respectively. Equation (8) is similar to that given in Danilov and Gurarie (2002) for a 2-D flow although it can also be applied in the case of 3-D flows. This is true if the injection rate

NPGD
1, 97–129, 2014

ε in Eq. (8) is modified to include the contribution of open boundary conditions (if any). Since ε was not determined for the CCS, the injection rate in Eq. (8) was not changed.

Nonlinear interactions are effective if $\Omega < \Gamma_m$ (Rabinovich and Trubetskov, 1989). For simplicity, we replace $\Gamma \sim \Gamma_m$ and with $\Omega = \gamma\, Rn$ then λ in the flow should be limited as

$$\lambda > \gamma^2 \Gamma^{-2} (\beta/2)^{-2} \varepsilon L^{-2}. \tag{9}$$

Since the value of the injection rate is not known (at least for the California Current System), this demonstrates only that there exists a threshold for Ω. Below this threshold, when the number of near-resonance quartets is strongly reduced as λ tends to zero, the energy transfer into QZJs should cease. The same conclusion can be made for BAOs as well.

So, QZJs require existence of some finite level of dissipativity. If this level is not reached, no zonal jets can be found in a flow. This conclusion agrees with results obtained by Berloff et al. (2011) who also found that jet generation requires existence of some finite level of dissipation in a system. Another issue is how the choice of dissipativity controls the latency of QZJs.

Chelton et al. (2007, 2011) have hypothesized that propagating SSH anomalies off California were a response of the ocean surface to mesoscale eddies because there is “practically” no wave dispersion for such scales. Estimates obtained in this study and Ivanov et al. (2010) have shown that wave dispersion is finite. Rossby waves of annual and semi-annual periodicities which participate in quartets are clearly dispersion waves at least in linear and quasi-linear regimes of propagation (Ivanov et al., 2010). They also participate in modulational instability. Therefore, these SSH anomalies should be interpreted as a result of forcing by nonlinear Rossby waves.

Note that bottom friction is very important for generation of broadening of the spectral peaks that correspond to waves. The point is that any turbulent process generates broadening of the peaks, and turbulence is always present in oceanic flows. The broadening of the peaks by turbulence is described in the Appendix of Galperin et al. (2010).

NPGD
1, 97–129, 2014

8 Phase synchronization/locking events

A number of mechanisms form QZJs in the ocean. QZJs can be generated by near-resonance triple interactions between modes (e.g., see Lee and Smith, 2007), anomalous local wind forcing, as assumed in Nakano and Hasumi (2005); or by the instability of background currents (e.g., Berloff et al., 2009). But in each of these cases, if nonlinear interactions including quartets play an important role, phase synchronization/locking events should be expected. These can be easily extracted from observations in phase space (Pikovsky et al., 2001).

The M-modes introduced by Eq. (1) generate an appropriate phase space. Hence, the underlying structure of quasi-zonal jets and inter-scale interactions forming these jets can be analyzed through the phase–frequency analysis of M-mode dynamics using amplitude–phase variables. Phase synchronization corresponds to the case when the phase difference between two oscillations is zero. Phase locking assumes this difference is constant (Pikovsky et al., 2001).

Using Eq. (2) does not solve the problem of phase synchronization/locking events because estimates have shown that in this case only the 1999–2001 phases can be observed. Therefore, another definition of phase synchronization/locking events based on Pereira et al. (2007) is used. They suggested that phase synchronization/locking events in a nonlinear system can be detected through correlations between local maxima and minima of system variables in phase space. In this study, amplitudes of M-modes were used as system variables. Two modes were in phase (anti-phase) if the difference between two times t_j and t_{j^*} corresponding to two neighboring maxima or two neighboring minima was less than some threshold δ, i.e.,

$$\left|t_j - t_{j^*}\right| \le \delta. \tag{10}$$

$\delta = 0$ corresponds to phase synchronization, and $\delta \neq 0$ is phase locking. Note that in comparison with traditional techniques for calculation of phase of a multi-frequency signal as a wavelet or Hilbert transform, the above approach is applicable to any signal that contains distinct marker events.

NPGD
1, 97–129, 2014

Appropriate histograms calculated as discussed above are shown in Fig. 9. It is clear from these histograms that quartets (four wave interacting structures) were detected in two different spectral bands. First, modes corresponding to QZJs, annual Rossby waves, semi-annual Rossby waves and MEs from the 5th spectral band formed quartets which were responsible for energy transfer from Rossby waves to the QZJs (Fig. 9a, c, e and g). These quartets corresponded to maximum values of η^2. The quasi-zonal jets had maximum lengths (long jets) when the number of synchronization events was maximum.

Second, modes which corresponded to BAOs (with scales from 2 to 3 yr) correlated with semi-annual Rossby waves and mesoscale eddies from the 5th and 6th spectral bands (Fig. 9b, d, f and h). In this case the energy was transferred from Rossby waves to BAOs. Forming BAOs from semi-annual Rossby waves demonstrated the possibility of inverse cascades of energy to accelerate this process. Again these quartets corresponded to maximum values of η^2. However, since BAOs are not QZJs, they cannot have maximum length when the number of synchronization/locking events was maximum. But modes forming these oscillations have maximum amplitudes too.

Note that QZJs and BAOs did not interact with one another over the length of the data record. However, this does not mean that these processes were linear.

9 Conclusions

Some evidence of a self-organized process in the CCS is given here. It occurred when QZJs and BAOs were formed due to near-resonance inter-scale interactions through modulational instability. The number of observed quartets was 10 times larger than the number of induced triads. As a consequence, SSH signal was transferred from annual and semiannual Rossby waves and mesoscale eddies to lower frequency current structures such as QZJs and BAOs. This example demonstrates modulational (Benjamin–Feir) instability in which the carrier wave is phase locked with the side bands.

NPGD
1, 97–129, 2014

Two types of quartets were observed off California. Quartets of the first type contained QZJs, annual Rossby waves, semi-annual Rossby waves and mesoscale eddies from the fifth spectral band. Note that the mesoscale eddy field was strongly smoothed by the AVISO team. Therefore, although the harmonics which participated in nonlinear interactions were identified more or less accurately, fluxes between harmonics have been shifted into the Rossby wave band.

The second type of quartets consisted of BAOs, semi-annual Rossby waves and mesoscale eddies from fifth and sixth bands. Energy transfer to BAOs from faster currents seems to be a novel phenomenon and has not been noted in modern oceanographic literature (Baldwin et al., 2001).

Note that it was found that BAOs did not interact with QZJs nonlinearly within the given observational series. However this does not mean that BAOs or QZJs should be approximately linear, although they are the lowest frequency currents observed in satellite data.

Dissipativity of an oceanic flow controls generation of QZJs and BAOs. This is because the level of dissipativity determined the number of near-resonances causing non-local energy transfer from fast to slower time scales (inverse time cascade). A minimum dissipativity level in the CCS was shown to exist (it was demonstrated for example, for bottom friction) when QZJs and BAOs were generated.

These results help in understanding a role of QZJs in the CCS. Although the QZJs have a considerably weaker signature in SSH anomalies than RWs, they acted as a catalyst, helping RWs, MEs and QZJs exchange energy between themselves. In our opinion, QZJs could not serve as barriers for meridional transport in the CCS because they are too weak.

Conclusions made in this paper apply only to the California Current System. Other physical mechanisms for generation of QZJs may exist in other regions. For example, Tanaka and Akitono (2010) found the existence of two different mechanisms in a two-layer model of an idealized ocean. Note that our analysis does not support Centurioni

NPGD
1, 97–129, 2014

et al. (2008), who discussed direct instability of the CCS meanders and hypothesized a possible mechanism of QZJ generation in this region as plumes.

Acknowledgements. Support for L. M. Ivanov (Curt Collins) was provided by NSF grant OCE-0827527 (OCE-0827160). The authors thank J. McWilliams (UCLA), E. Pelinovsky (Institute of Applied Physics, Russia) and B. Galperin (University of South Florida) for useful discussions of these results.

References

Aubry, N., Guyonett, R., and Lima R.: Spatio-temporal analysis of complex signals: theory and applications, J. Stat. Phys., 64, 683–739, 1991.

Baldwin, M. P., Gray, L. G., Dunkerton, T. J., Hamilton, K., Haynes, P. H., Randel, W. J., Holton, J. R., Alexander, M. J., Hirota, I., Horinouchi, T., Jones, D. B. A., Kinnersley, J. S., Marquardt, C., Sao, K., and Takahasi, M.: The Quasi-Biennial Oscillation, Rev. Geophys., 39, 179–229, 2001.

Baldwin, M. P., Rhines, P., Huang, H.-P., and McIntyre, M.: The jet-stream conundrum, Science, 315, 467–468, 2007.

Berloff, P., Kamenkovich, I., and Pedlosky, J.: A mechanism of formation of multiple zonal jets in the oceans, J. Fluid Mech., 628, 3950-425, 2009.

Berloff, P., Karabasov, S., Farrar, T., and Kamenkovich, I.: On latency of multiple zonal jets in the oceans, J. Fluid. Mech., 686, 534–567, 2011.

Castelao, R. M., Mavor, T. P., Barth, J. A., and Breaker, L. C.: Sea surface temperature fronts in the California Current System from geostationary satellite observations, J. Geophys. Res., 111, C09026, doi:10.1029/2006JC003541, 2006.

Centurioni, L. R., Ohlman, J. C., and Niiler,P. P.: Permanent meanders in the California Current System, J. Phys. Oceanogr., 38, 1690–1710, 2008.

Chelton, D. B., Schlax, M., and Samelson, R. M.: Global observations of nonlinear mesoscale eddies, Prog. Oceanogr., 91, 167–216, 2011.

Chu, P. C., Ivanov, L. M., Korzhova, T. P., Margolina, T. M., and Melnichenko, O. V.: Analysis of sparse and noisy ocean current data using flow decomposition, Part 1, J. Atmos. Ocean Tech., 20, 478–491, 2003.

Collecte Localisation Satellites, SSALTO/DUACS user handbook: (M) SLA and (M) ADT near-real time and delayed time products, CLS-DOS-NT-06.034, Ramonville Saint-Agne, France, 54 pp., 2006.

Connaugton, C., Nadiga, B., Nazarenko, S., and Quinn, B.: Modulational instability of Rossby and drift waves and generation of zonal jets, J. Fluid Mech., 654, 207–231, 2010.

Danilov, S. and Gurarie G.: Rhines scale and spectra of the β-plane turbulence with bottom drag, Phys. Rev. E, 65, 067301-1–067301-3, 2002.

Dritschell, D. G. and Scott, R. K.: Jet sharpening by turbulent mixing, Philos. Tran. A, 369, 754–778, 2011.

Galperin, B., Sukoriansky, S., and Dikovskaya N.: Geophysical flows with anisotropic turbulence and dispersive waves: flows with a beta-effect, Ocean. Dynam., 60, 427–441, 2010.

Gill, A. E.: The stability of planetary waves on an infinitie beta-plane, Geophys. Fluid Dynam., 6, 29–47, 1974.

Hristova, H., Pedlosky, J., and Spall, M. A.: Radiating instability of meridional boundary current, J. Phys. Ocean., 38, 2294–2307, 2008.

Ivanov, L. M. and Collins, C. A.: Modal decomposition of oceanic circulation: Applications for high-resolution models and Lagrangian data, in: Chapter 2, Ocean Circulation and El Niño, New Research Nova Science Publishers, Inc., New York, 31–69, 2009.

Ivanov, L. M., Collins, C. A., and Margolina, T. M.: System of quasi-zonal jets off California revealed from satellite altimetry, Geophys. Res. Lett., 36, L03609, doi:10.1029/2008GL036327, 2009.

Ivanov, L. M., Collins, C. A., Margolina, T. M., and Eremeev, V. N.: Nonlinear Rossby waves off California. Geophys. Res. Lett., 37, L13602, doi:10.1029/2010GL043708, 2010.

Ivanov, L. M., Collins, C. A., and Margolina, T. M.: Detection of quasi-zonal jets in ocean from altimetry observations, J. Atmos. Ocean. Tech., 29, 111–126, 2012a.

Ivanov, L. M., Collins, C. A., and Margolina, T. M.: Jets, Rossby Waves and Eddies off California, in Proc.: 20 Years of Progress in Radar Altimery, Venice, 46–52, 2012b.

Jacobs, G. A., Emery, W. J., and Born, G. H.: Rossby waves in the Pacific Ocean extracted from Geosat altimetry data, J. Phys. Oceanogr., 1155–1175, 1993.

Jacobs, G. A., Teaque, W. J., Mitchell, J. L., and Hurlburd, H. E.: An examination of the North Pacific Ocean in the spectral domain using Geosat altimeter data and a numerical ocean model, J. Geophys. Res., 101, 1025–1044, 1996.

NPGD
1, 97–129, 2014

On modulation instability in a system of jets, waves and eddies off California

L. M. Ivanov et al.

Kartashova, E., Lvov, V., Nazarenko, S., and Procaccia, I.: Towards a Theory of Discrete and Mesoscopic Wave Turbulence, Technical report no. 10-04 in RISC Report Series, Research Institute for Symbolic Computation, 2010.
Kumar, P. and Foufoula-Georgiou, E.: Wavelet analysis for geophysical applications, Rev. Geophys., 34, 385–412, 1997.
Laskar, J.: Frequency analysis for multi-dimensional systems, Global dynamics and diffusion, Physica D, 67, 257–281, 1993.
Lee, Y. and Smith, L. S.: On the formation of geophysical and planetary zonal flows by near-resonance wave interactions, J. Fluid Mech., 576, 405–424, 2007.
Loesch, A. Z.: On generation of zonal flows by interacting Rossby waves, Tellus, 29, 306–316, 1977.
Lorenz, E. N.: Barotrophic instability of Rossby wave motion, J. Atmos. Sci., 29, 258–264, 2007.
Manfredi, G., Roach, C. M., and Dendy, R. O.: Zonal flow and streamer generation in drift turbulence, Plasma Phys. Control. Fusion, 43, 825–835, 2001.
Moffatt, H. K.: Magnetic Field Generation in Electrically Conducting Fluids, Cambridge University Press, 578 pp., 1978.
Nadiga, B.: On zonal jets in oceans, Geophys. Res. Lett., 33, L10601, doi:10.1029/2006GL025865, 2006.
Nakano, H. and Hasumi H.: A series of zonal jets embedded in broad zonal flows in the Pacific obtained in eddy-permitting ocean general circulation models, J. Phys. Oceanogr., 35, 474–488, 2005.
Newell, A.: Rossby wave packet interactions, J. Fluid. Mech., 35, 255–271, 1969.
Nicolis, G. and Prigogine, I.: Self-Organization in Non-Equilibrium Systems, Wiley, New York, 1977.
Pedlosky, J.: Geophysical Fluid Dynamics, 2nd Edn., Springer, New York, 625 pp., 2007.
Pereira, T., Baptista, M. S., and Kurths, J.: Detecting phase synchronization by locates maps: Application to neural networks, Eur. Phys. Lett., 77, 40006, doi:10.1209/0295-5075/77/40006, 2007.
Pikovsky, A., Rosenblum, M., and Kurths, J.: Synchronization: A Universal Concept of Nonlinear Sciences, Cambridge Press, 2001.
Rabinovich, M. I. and Trubetskov, D. I.: Oscillations and Waves: In Linear and Nonlinear Systems, Springer Verlag, Berlin, 1989.
Rhines, P. B.: Wave s and turbulence on beta-plane, J. Fluid Mech., 69, 417–443, 1975.

NPGD
1, 97–129, 2014

Rhines, P. B.: Rossby Waves, Academic Press, Salt Lake City, 1–37, 2002.
Rhines, P. B.: Oceanic and Atmospheric Rossby Waves, Norman Phillips Symposium at the Annual meeting of the American Meteorological Society, Boston, 41 pp., 2004.
Schlax, M. G. and Chelton, D. B.: The influence of mesoscale eddies on the detection of quasi-zonal jets in the ocean, Geophys. Res. Lett., 35, L24602, doi:10.1029/2008GL035998, 2008.
Srinivasan, K. and Young, W. R.: Zonostrophic instability, J. Atmos. Sci., 69, 1633–1656, 2012.
Tanaka, Y. and Akitomo, K.: Alternating zonal flows in a two-layer wind driven ocean, J. Oceanogr., 66, 475–487, 2010.
Vallis, G. K. and Maltrud, M. E.: Generation of mean flows and jets on a beta plane and over topography, J. Phys. Oceanogr., 23, 1346–1362, 1993.
Wang, J., Spall, M. A., Flierl, G. R., and Malanotte-Rizzole, P.: A new mechanism for the generation of quasi-zonal jets in the ocean, Geophys. Res. Lett., 39, L10601, doi:10.1029/2012GL051861, 2012.

NPGD
1, 97–129, 2014

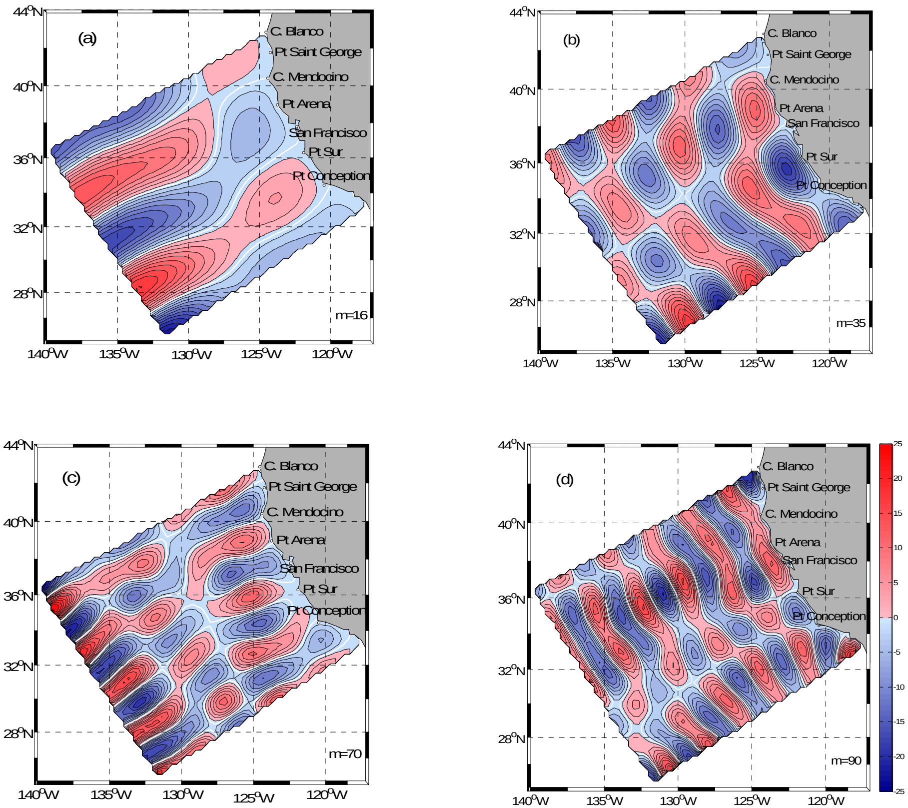

Fig. 1. Structure of basis functions (M-modes, $\Psi_m \times 10^5$) used for calculations. **(a)** $m = 16$, **(b)** $m = 35$, **(c)** $m = 70$, and **(d)** $m = 90$. White contours are zero isolines.

NPGD
1, 97–129, 2014

On modulation instability in a system of jets, waves and eddies off California

L. M. Ivanov et al.

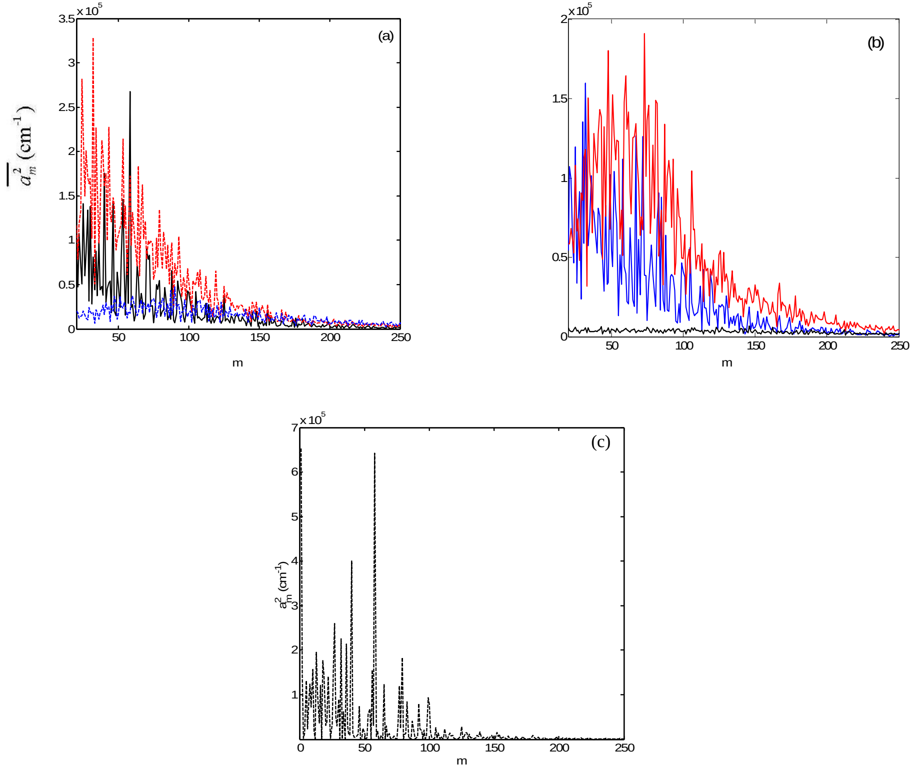

Fig. 2. Spectral characteristics of coherent structures observed off California. **(a)** and **(b)** Time averaged energy density ($\overline{a_{\mathrm{m}}^2}$) vs. mode number for the six frequency bands used in this study. **(a)** Black, red and blue correspond to quasi-zonal jets (with scales longer than 36 months), annual Rossby waves (with scales from 8 to 18 months), and mesoscale eddies (with scales from 2 to 4 months). **(b)** Blue, red and black correspond to bi-annual oscillations (with scales from 18 to 36 months), semi-annual Rossby waves (with scales from 4 to 8 months), and mesoscale eddies (with scales from 1 to 2 months). **(c)** An instanteous spectrum a_{m}^2.

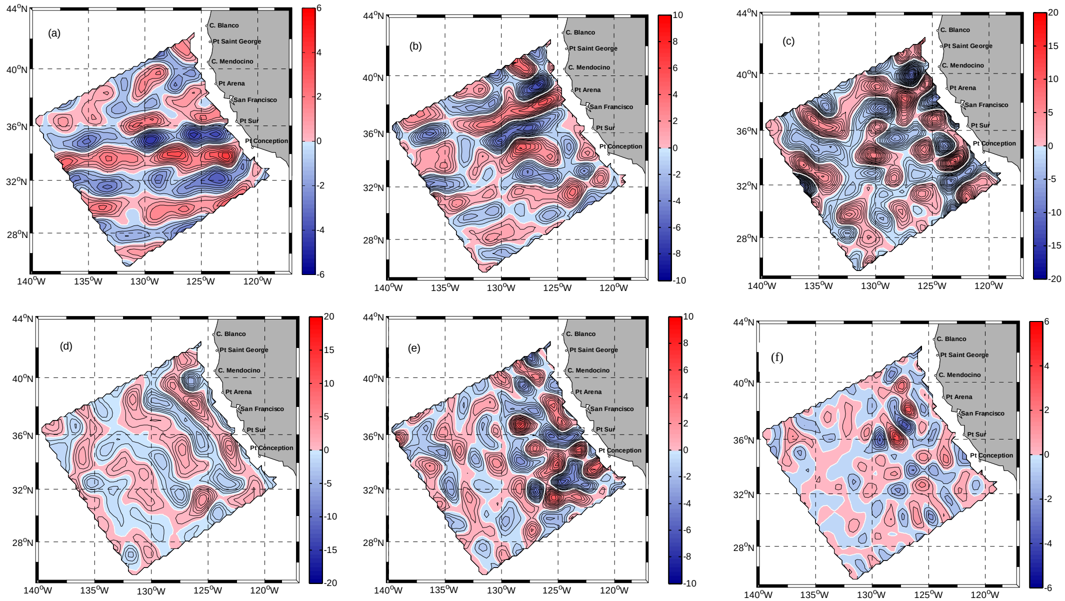

Fig. 3. Characteristic spatial structure of **(a)** quasi-zonal jets (26 May 2006); **(b)** bi-annual oscillations (11 January 2006), **(c)** annual Rossby waves (4 October 2006), **(d)** semi-annual Rossby waves (28 November 2007); **(e)**, **(g)** mesoscale eddies (22 November 2006 and 9 May 2006). Contour intervals are 1 and 0.5 cm in **(a)**–**(d)** and **(e)** and **(f)**, respectively. Note that the range of the contours varies from ±6 in **(a)**, **(g)** to ±10 in **(b)**, **(e)** and ±20 in **(c)**, **(d)**.

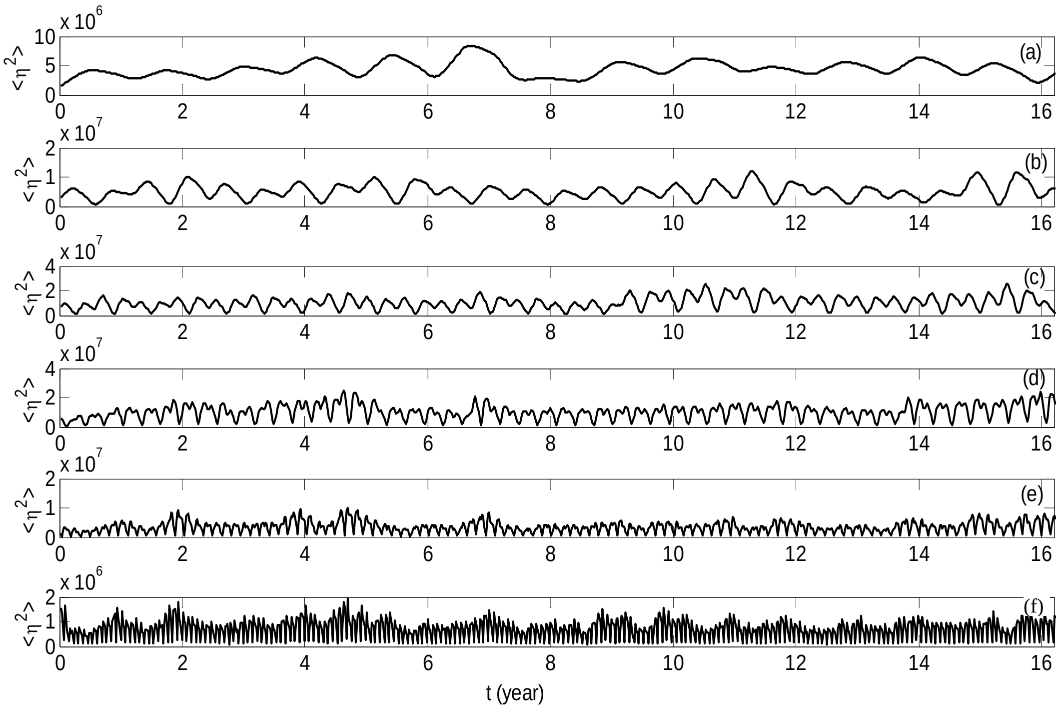

Fig. 4. Temporal behavior of $\left\langle \eta^2 \right\rangle$ (cm^2) for six spectral bands: **(a)** longer than 6 months, quasi-zonal jets; **(b)** 18 to 36 months, biannual oscillations; **(c)** 8 to 18 months, annual Rossby waves; **(d)** 4 to 8 months, semiannual Rossby waves; **(e)** 2 to 4 months, mesoscale eddies; and **(f)** 1 to 2 months, mesoscale eddies.

NPGD
1, 97–129, 2014

On modulation instability in a system of jets, waves and eddies off California

L. M. Ivanov et al.

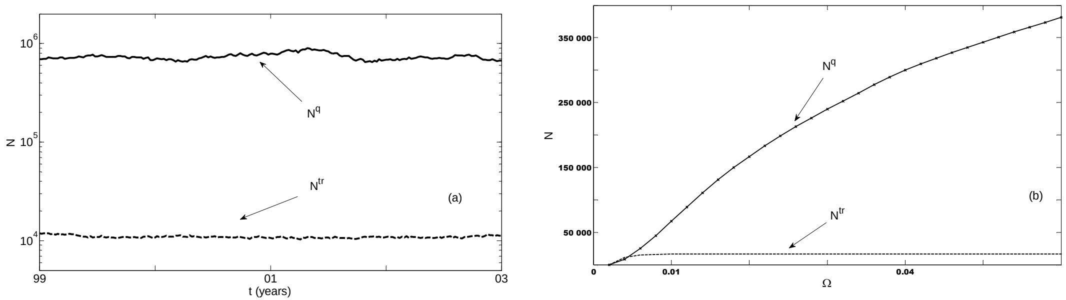

Fig. 5. Variability of the number of near resonance triplets, N^{tr}, and near resonance quartets, N^q, as a function of **(a)** time and **(b)** resonance broadening, Ω.

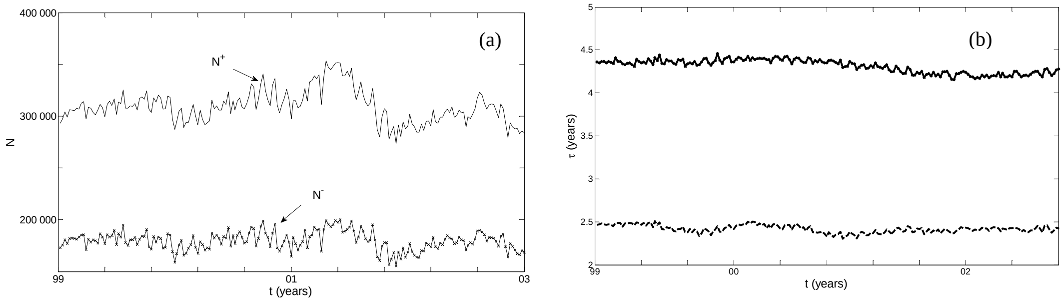

Fig. 6. Temporal behavior of the number and time scale of near resonance quartets corresponding to for quasi-zonal jets and biannual oscillations in 1999–2003. **(a)** Number of near resonance quartets which participated in inter-scale interactions to generate the energy for quasi-zonal jets (QZJs) (N^+) and biannual oscillations (BAOs) (N^-). **(b)** Mean time scales for QZJs (–) and BAOs (–).

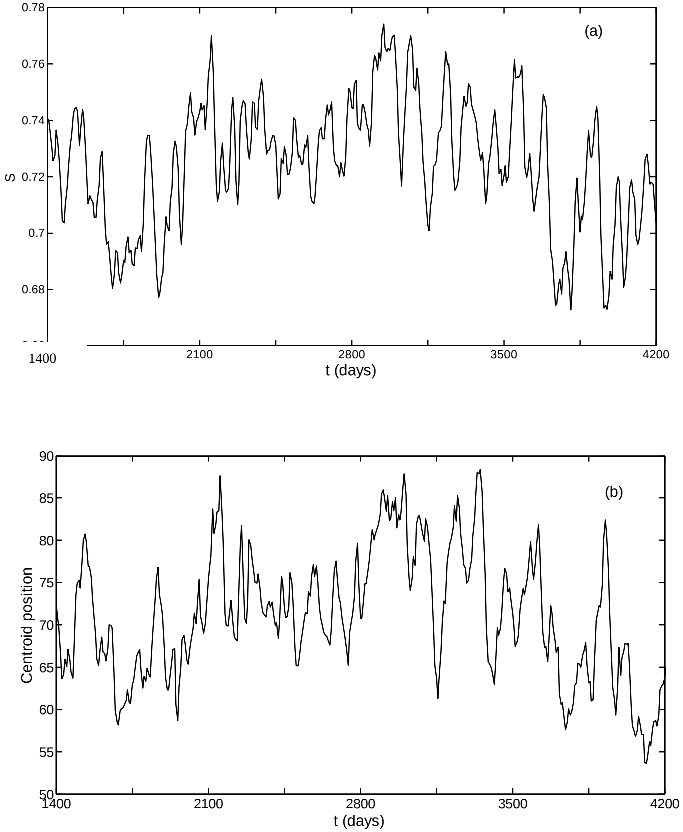

Fig. 7. Evolution of spectral entropy and centroid, 10 October 1992 to 23 May 2009. **(a)** Spectral entropy in non-dimensional units. **(b)** Spectral centroid in m.

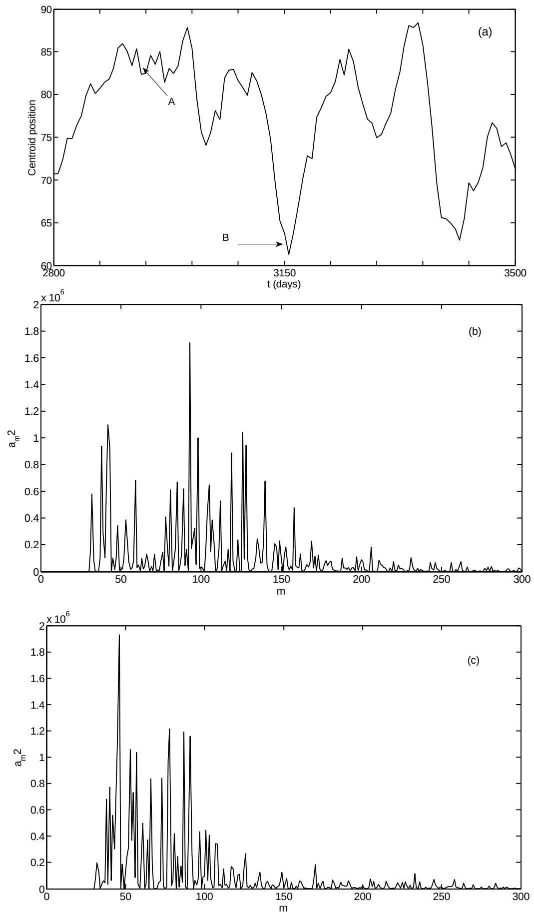

Fig. 8. An evolution of the spectral centroid. **(a)** Spectral centroid, from 5 August 1999 to 5 July 2000. A and B indicate a time interval within which the centroid moved to lowest value. **(b)** Spectrum of a_m^2 for point A on 2940 day. **(c)** Spectrum of a_m^2 for point B on 3150 day.

NPGD
1, 97–129, 2014

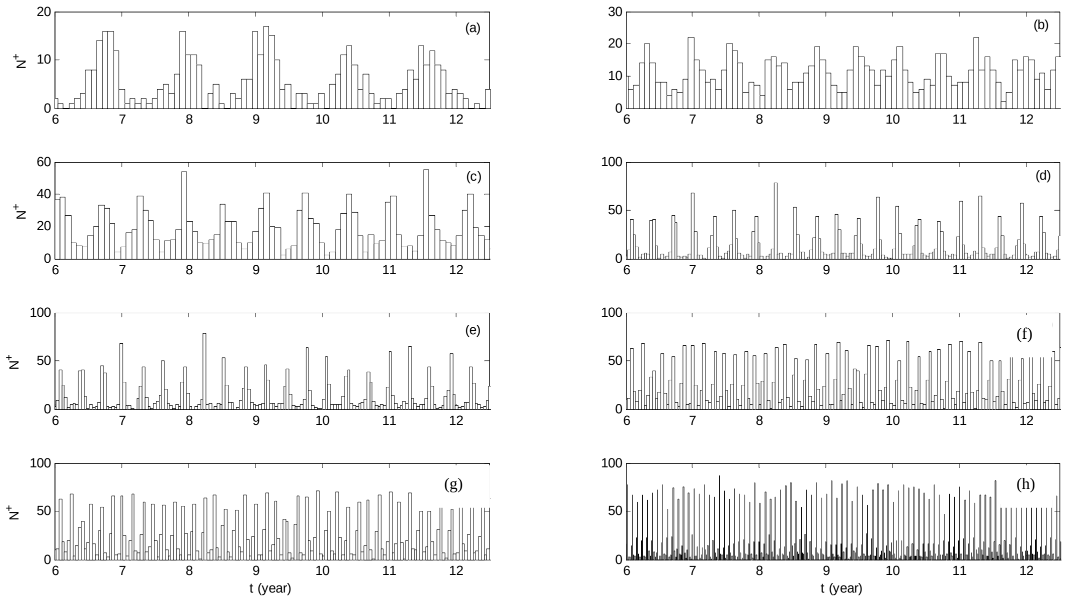

Fig. 9. Synchronization/locking events off California. **(a)** The first quartets among the quasi-zonal jets, annual Rossby waves, semiannual Rossby (SARWs) waves and mesoscale eddies from the fifth band; **(b)** the second quartets formed by biannual oscillations, SARWs and mesoscale eddies from the fifth and six spectral bands. N^+ is a number of synchronized modes.

NPGD
1, 97–129, 2014